Journal of Electroanalytical Chemistry 807 (2017) 181–186

Contents lists available at ScienceDirect

Journal of Electroanalytical Chemistry

journal homepage: www.elsevier.com/locate/jelechem

Nanostructuring of anodic copper oxides in fluoride-containing ethylene glycol media

Diego P. Oyarzún Jerez[a,*], Manuel López Teijelo[b], Wilkendry Ramos Cervantes[b], Omar E. Linarez Pérez[b,*], Julio Sánchez[c], Guadalupe del C. Pizarro[d], Gabriela Acosta[e], Marcos Flores[e], Ramiro Arratia-Perez[a]

[a] Center of Applied Nanosciences (CANS), Facultad de Ciencias Exactas, Universidad Andrés Bello, Avenida República 275, Santiago, Chile
[b] Instituto de Investigaciones en Fisicoquímica de Córdoba (INFIQC), Facultad de Ciencias Químicas, Universidad Nacional de Córdoba, Haya de la Torre y Medina Allende, 5000 Córdoba, Argentina
[c] Departamento de Ciencias del Ambiente, Facultad de Química y Biología, Universidad de Santiago de Chile, USACH, Casilla 40, Correo 33, Santiago, Chile
[d] Laboratorio de Polímeros y Ciencia de los Materiales, Departamento de Química, Universidad Tecnológica Metropolitana, Avda. Las Palmeras 3360, Santiago, Chile
[e] Laboratory of Surface and Nanomaterials, Physics Department, Faculty of Physics and Mathematics Science, Universidad de Chile, Beauchef 850, Santiago, Chile

ARTICLE INFO

Keywords:
Copper oxides
Nanostructured oxides
Raman
XPS

ABSTRACT

We demonstrate that the anodization of copper in alkaline water/ethylene glycol media containing fluoride ions generates nanostructured copper oxide films. By modifying the anodization conditions (fluoride and OH^- concentrations, applied voltage and anodization time), nanofibrillar Cu_2O as well as highly rough nanofibrillar network or nanoporous mixed Cu_2O/CuO films are obtained. Raman and X-ray Photoemission Spectroscopy (XPS) results indicate that in fluoride presence, Cu(I) oxide is obtained when anodization takes place applying low voltages at a relatively low OH^- concentration. In comparison, the subsequent oxidation to obtain Cu(II) species (CuO and $Cu(OH)_2$) is promoted by increasing the OH^- contents. According to the present results, an oxidation reaction scheme is proposed in order to gain a deeper understanding in the preparation of controlled nanostructured copper oxide films.

1. Introduction

Nowadays, the preparation and characterization of nanostructured materials have an increasing interest because of their novel properties and potential applications in diverse areas such as medicine, optoelectronics, acoustics, photonics, sensors and catalysis [1–4]. Nanostructures can be prepared in various geometries as wires, rods, spheres, pores and tubes, among others, either individually differentiated or as a part of films. This, in turn, generates high-surface area materials that could improve the performance of luminescent modules, piezoelectric transducers, semiconductor electrodes, chemical sensors and electrocatalysts [3,5,6].

Within semiconducting materials, nanostructured copper oxides (p-type semiconductors) are very promising for use in different applications mainly due to their low cost, non-toxic nature, and low bandgap values ($E_g(Cu_2O)$ = 2.17 eV and $E_g(CuO)$ = 1.2–1.9 eV). These properties turn Cu_2O into a favorable material for the design of solar cells, LEDs, as well as in water photolysis, which is favored due to the fact that conduction and valence bands are near to the water reduction and oxidation potentials [7–9].

Several synthesis methods for Cu_2O, CuO and $Cu(OH)_2$ nanostructures have been reported, e.g. thermal oxidation of metallic copper at high temperatures, template assisted growth, colloidal methods, electron-beam evaporation and sputtering, and electrochemical anodization [9–20]. High-temperature processes limit the control over the interfacial characteristics of the thin films, which significantly affect the optical and photoelectrochemical properties of the resulting oxides. In addition, the use of templates and colloidal synthesis methods leads to low adherence over conducting substrates, limiting their use or integration into electronic devices. On the other hand, electrochemical anodization has been successfully used to synthesize a wide variety of nanostructures. The preparation of copper oxide films by anodization techniques offers potential advantages in relation to their integration in electronic devices.

Several reports on the electrochemical preparation of Cu oxide/hydroxide nanostructures are found in the literature, but the oxidation mechanisms have not been fully elucidated yet. Wu et al. [16] obtained $Cu(OH)_2$ nanotubes and nanoneedles, with their morphology being

* Corresponding authors.
E-mail addresses: diego.oyarzun@unab.cl (D.P. Oyarzún Jerez), olinarez@unc.edu.ar (O.E. Linarez Pérez).

https://doi.org/10.1016/j.jelechem.2017.11.047
Received 19 September 2017; Received in revised form 14 November 2017; Accepted 15 November 2017
Available online 16 November 2017
1572-6657/

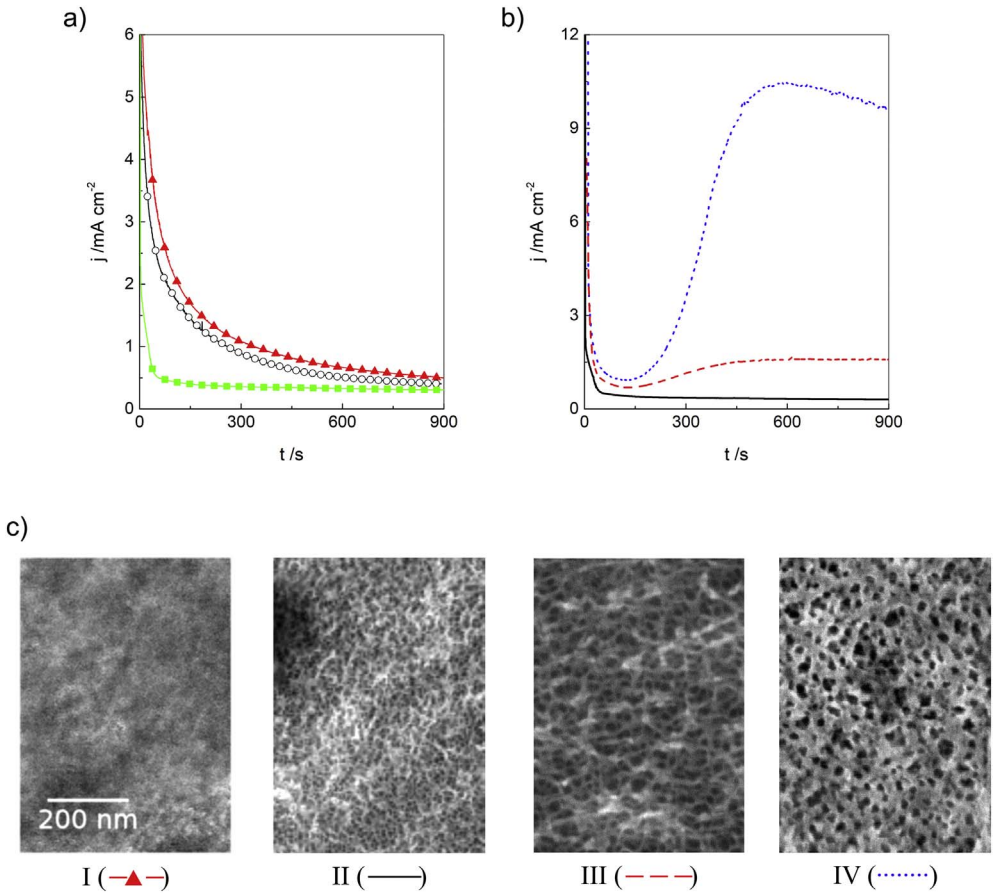

Fig. 1. Potentiostatic j/t profiles (a–b) and final morphology (c) for Cu foils anodized applying different voltages (E_{ap}) during 15 min at 5 °C in a 0.1 M KOH and 1% v/v H_2O in ethylene glycol containing x % w/v NH_4F electrolyte.
a) E_{ap} = 5 V and x: 0 (–▲–); 0.01 (–○–); 0.1 (–■–).
b) x = 0.1% and E_{ap}: 5 V (– – –); 10 V (— — —); 20 V (·····).
c) x = 0% and E_{ap} = 5 V (I); x = 0.1% and E_{ap}: 5 V (II); 10 V (III); 20 V (IV).

controlled by the electrolyte composition, pH and applied voltage. They also demonstrated that $Cu(OH)_2$ can be successfully transformed into CuO by a suitable thermal treatment, thus resulting in a simple, clean and efficient route for the manufacture of nanostructured $Cu(OH)_2$ or CuO films. In addition, Duc-Duong et al. [17] obtained Cu_2O nanowires presenting a preferential direction of growth in the plane [100] by applying a density current of 2 mA cm^{-2} in 1 M NaOH at 20 °C. They found that the wire diameter and length depend on pH, but that no changes in the composition and crystalline structure take place. On the other hand, Sahoo et al. [18] prepared different Cu_2O nanostructures via the anodization of $Cu/SiO_2/Si$ substrates in deionized water, which show interesting photon sensing characteristics under white light illumination. Recently, Allam et al. [19] obtained laminar Cu_2O nanostructures, with thickness up to 500 nm, and highly porous Cu_2O films using chloride and fluoride salts in non-aqueous electrolytic media, similar to those used for the controlled growth and preparation of nanoporous and nanotubular TiO_2 structures [6,21,22].

This work aims at understanding the chemical processes involved during the anodization of copper in alkaline water/ethylene glycol media containing fluoride ions, to successfully obtain specific nanostructures. The dependence of the morphology and chemical composition of the anodized copper surfaces were correlated to the experimental conditions (applied voltage, fluoride and hydroxyl concentrations, and anodization time). The morphology was studied using field-emission scanning electron microscopy (FESEM) and the chemical composition by means of Raman and X-Ray photoemission spectroscopy (XPS).

2. Experimental section

Copper anodization was performed in an electrochemical cell with a two-electrode configuration. The anode electrodes consisted of polycrystalline copper foils (Sigma Aldrich, 99.99% purity) of 250 μm in thickness (0.5 cm^2 of exposed geometric area) mounted in Teflon holders. A 0.5 cm thickness graphite sponge of 3.0 × 3.5 cm^2 was used as cathode electrode. Prior to anodization, the samples were mechanically polished using a 0.05 μm alumina aqueous suspension and then, degreased by sonication in a 50:50 acetone/ethanol mixture for 15 min. After cleaning, the foils were rinsed with deionized water and dried under N_2 flux. High-voltage anodization experiments were carried out using a 173 EG&G PAR potentiostat/galvanostat coupled to a 175 EG&G PAR signal generator and a 7090A Hewlett Packard plotting recorder. The anodic growth of the copper oxide films was performed by applying a potential pulse up to different voltage values (E_{ap}) in the range of 5–20 V for different anodizing times (t_a) at 5 °C with continuous stirring. The electrolytic solutions were prepared from analytical grade reagents and were based on ethylene glycol; 1% v/v water; x % w/v ammonium fluoride ($0 \leq x \leq 0.1$) and yM KOH ($0.1 \leq y \leq 0.5$).

The morphology features of the nanostructured layers were characterized by field emission scanning electron microscopy (FE-SEM) using a Carl Zeiss Σigma microscope. Raman experiments were performed ex situ (in air) using a Horiba LabRAM HR spectrometer, employing a He/Ne laser (632.8 nm wavelength). X-ray photoelectron spectroscopy (XPS) was used to determine the chemical states of the samples. A XPS-Auger Perkin Elmer electron spectrometer Model PHI 1257 running in an ultra-high vacuum chamber with hemispherical electron energy analyzer, was used. The X-ray source, which provided unfiltered Kα radiation, consisted of an Al anode ($h\nu$ = 1486.6 eV). The pressure of the main spectrometer chamber during data acquisition was maintained at ca. 10^{-7} Pa. The binding energy (BE) scale was calibrated using the peak of adventitious carbon, which was set to 284.8 eV. The recorded HRXPS signal was fitted by using CASA software, and the species composition was calculated taking into account

the integrated area under each curve, the full width at half maximum (FWHM), and the corresponding atomic sensitivity factors (ASF).

3. Results

Fig. 1 shows the potentiostatic j/t profiles (a,b) and final morphology (c) for Cu foils anodized applying different voltages (E_{ap}) during 15 min at 5 °C, in a 0.1 M KOH + 1% v/v H_2O in ethylene glycol containing x % w/v NH_4F electrolyte. For all the conditions employed (Fig. 1a and b), initially the current density increases sharply due to the active dissolution of the copper substrate ($Cu \rightarrow Cu^{n+} + ne^-$). Afterwards, the current density decreases significantly, indicating that passivation of the electrode surface due to the growth of a low-conducting layer takes place. For 5 V, as the fluoride concentration increases from 0 to 0.1% w/v, the density current values diminishes (Fig. 1a) and a morphologic transition from almost smooth to a fibrillary textured surface, (Fig. 1c-I and c-II) is obtained. On the other hand, in the presence of 0.1% w/v of fluoride (Fig. 1b) and increasing the applied voltage from 5 to 20 V, the j/t profiles show a minimum at around 150 s followed by an increase in the current values that is more marked as the applied voltage increases, reaching finally a quasi-steady state current. This response is attributed to a marked increase in roughness promoted by the film chemical dissolution due to the presence of fluoride. A morphologic evolution from nanofibrillar to a noticeably nanoporous surface (Fig. 1c-II to IV) is also noticeable. For E_{ap} = 20 V (Fig. 1c-IV), The pores are randomly distributed (Fig. 1c-II to IV) and their average diameter, which increase with the applied potential, are 6 ± 1 nm; 10 ± 2 nm and 15 ± 6 nm for 5, 10 and 20 V, respectively. A similar behavior has also been observed for other metals as titanium during anodization in fluoride-containing media [6,21,22], where nanopore/nanotubular structures are obtained. Even though the anodic TiO_2 film grows by a different mechanism, after a compact and/or porous oxide layer is formed, the competition between oxide formation and film dissolution to give soluble species takes place and parameters such as fluoride and water content as well as applied potential determine the nanostructure obtained.

In order to elaborate a detailed analysis about the copper chemical state and the film composition, Raman and XPS measurements were performed. For the non-fluoride containing electrolyte (Fig. 2-I), the signals at 296 cm^{-1} (sharp), 343 cm^{-1} (low intensity), and the wide band around 600–635 cm^{-1} are attributed to the presence of CuO species, as previously reported for aqueous electrolytes [23–25]. Additionally, the absence of a characteristic band at 488 cm^{-1} indicates no evidence of $Cu(OH)_2$ on the sample [23]. On the contrary, when fluoride ions are incorporated to the electrolytic bath (Fig. 2-II to IV), the Raman spectra show well-defined Cu_2O features: a signal at 150 cm^{-1} and two broad bands at 537 cm^{-1} and 620 cm^{-1} [23–25]. In addition, for E_{ap} = 20 V (Fig. 2-IV), an incipient signal at 300 cm^{-1} is also observed, indicating a minor presence of CuO at the anodized copper surface. Table 1 summarizes the morphologies obtained for the different conditions as well as Raman assignments.

Fig. 3 shows the $Cu2p_{3/2}$ (a,d), Cu LMM (b,e) and O1s (c,f) HRXPS spectra for Cu foils anodized applying 5 V (15 min) and 20 V (3 min) at 5 °C in a 0.1 M KOH and 1% v/v H_2O in ethylene glycol containing 0.1% w/v NH_4F electrolyte. Because of the overlapping between metallic Cu and Cu_2O lines in the $Cu2p_{3/2}$ region, and the metallic Cu with CuO in the Cu Auger LMM band, for the chemical assignments both binding energy regions were analyzed complementarily [14].

For the Cu sample anodized at 5 V, the high resolution $Cu2p_{3/2}$ spectrum recorded shows a well-defined symmetric peak (Fig. 3a). The fit was carried out taking into account a single contribution centered at a binding energy of 933.2 eV, which is associated to the underlying metallic Cu and the Cu_2O film [14,15]. Additionally, Cu LMM band (Fig. 3b) shows five contributions at 565.4; 568.1; 570.1; 571.0 and 574.7 eV. However, three of them (565.4; 571.0 and 574.7 eV) represent different transitions states of the Auger LMM and are neglected for the present analysis [14]. The other two bands centered at 570.2 eV and 568.1 eV are assigned to the Cu_2O (69%) and Cu + CuO (31%) species, respectively. According to the $Cu2p_{3/2}$ data (Fig. 3a), the band at 568.1 eV can be entirely assigned to the underlying Cu surface. In addition, the O1s signals (Fig. 3c) show three contributions at 530.6 eV (63%); 531.9 eV (34%) and 533.5 eV (3%), assigned to the Cu_2O, adsorbed OH^- and H_2O, respectively [14,15]. Besides, the signal at 530.5 eV may contain CuO contributions, but as the $Cu2p_{3/2}$ only shows

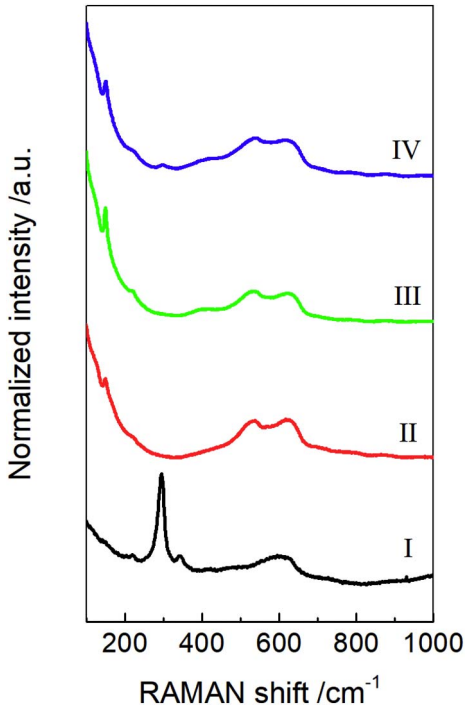

Fig. 2. Raman spectra for Cu foils anodized applying different voltages (E_{ap}) during 15 min at 5 °C in a 0.1 M KOH and 1% v/v H_2O in ethylene glycol containing x % w/v NH_4F electrolyte. x = 0% and E_{ap} = 5 V (I); x = 0.1% and E_{ap} = 5 V (II); 10 V (III); 20 V (IV).

Table 1
Morphologies as well as Raman shifts and XPS binding energies (BE) for Cu foil anodized applying 5, 10 and 20 V during different anodization times (t_a) at 5 °C in a yM KOH and 1% v/v H_2O in ethylene glycol containing 0.1% w/v NH_4F electrolyte.

		0.1 M KOH		0.5 M KOH
		5 V (15 min)	20 V (3 min)	10 V (6 min)
Film morphology		Nanofibrillar	Nanoporous	Highly rough nanofibrillar network
Raman shift/ cm^{-1}	Cu_2O	149.1; 537.8; 621.1	144.5; 542.0; 623.2	144.5; 538.3; 620.7
	CuO	–	289.9 (very low)	296.0; 345.7
	$Cu(OH)_2$	–	–	–
BE $Cu2p_{3/2}$/eV	Cu + Cu_2O	933.2 (100%)	932.5 (44%)	933.2 (64%)
	CuO	–	933.8 (24%)	934.2 (17%)
	$Cu(OH)_2$	–	935.5 (20%)	935.4 (13%)
	CuF_2	–	937.0 (12%)	–
BE Cu LMM/ eV	Cu_2O	570.2 (69%)	569.6 (80%)	570.2 (56%)
	Cu + CuO	568.1 (31%)	567.2 (20%)	568.4 (44%)
BE O1s/eV	Cu_2O + CuO	530.6 (63%)	530.1 (21%)	530.5 (22%)
	$Cu(OH)_2$ + OH^-	531.9 (34%)	531.5 (29%)	531.7 (58%)
	H_2O	533.5 (3%)	532.9 (50%)	532.9 (20%)
CuO/Cu_2O (*)		0	~0.3	~0.5

(*) estimated from $Cu2p_{3/2}$ line and Cu LMM bands according to ref. [14]

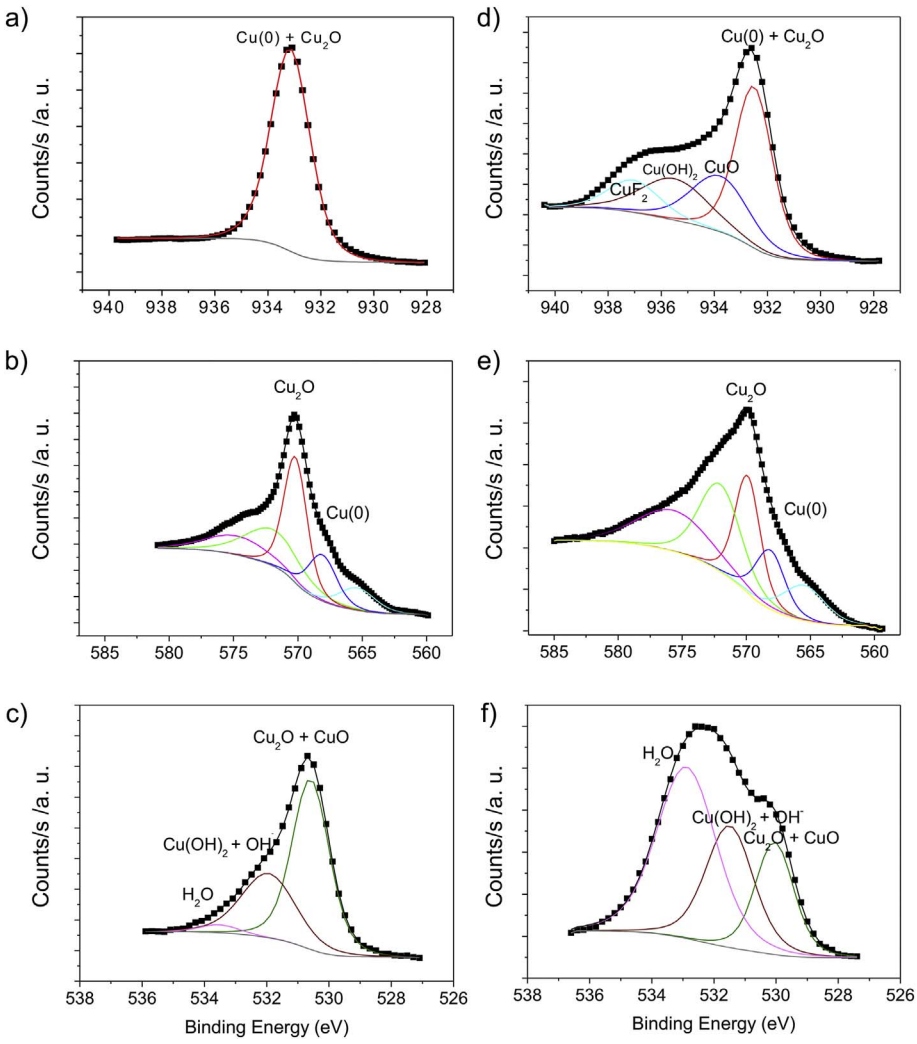

Fig. 3. $Cu2p_{3/2}$ (a,d), Cu LMM (b,e) and O1s (c,f) HRXPS spectra for Cu foils anodized applying 5 V during 15 min (a–c) and 20 V during 3 min (d–f) at 5 °C in a 0.1 M KOH and 1% v/v H_2O in ethylene glycol containing 0.1% w/v NH_4F electrolyte.

the Cu_2O contribution, an unambiguous assignation for this sample was made. These observations agree with the Raman experiments shown in Fig. 2(II and IV), which indicate that Cu_2O is the main species obtained after copper anodization at 5 V in alkaline water/ethylene glycol containing fluoride electrolyte.

On the other hand, after the anodization at 20 V, $Cu2p_{3/2}$ (Fig. 3d), Cu LMM (Fig. 3e) and O1s (Fig. 3f) signals show more complex features. For $Cu2p_{3/2}$, the fit was performed using four contributions centered at 932.5 eV (44%); 933.8 eV (24%); 935.5 (20%) and 937.0 eV (12%), which are assigned to metallic Cu surface and Cu_2O layer, CuO species, $Cu(OH)_2$, and CuF_2, respectively [14,15,27]. For the Cu LMM Auger bands (Fig. 3e), the peaks for Cu_2O at 569.6 (80%) and Cu + CuO at 567.2 (20%), are obtained. Furthermore, the fit of the O1s signals (Fig. 3f) shows the same oxygen contributions mentioned before: CuO and Cu_2O at 530.1 eV (21%); $Cu(OH)_2$ and adsorbed OH^- at 531.5 eV (29%), and adsorbed water at 532.9 eV (50%). Using the methodology described by Platzman et al. [14] for the precise separation of metallic Cu and CuO intensities from the $Cu2p_{3/2}$ line and Cu LMM bands neglecting $Cu(OH)_2$ contributions, a $CuO/Cu_2O \approx 0.3$ ratio for the XPS penetration depth ($^{<}$10 nm) was estimated (see Supporting information). These results indicate that for the higher applied voltages (20 V), a porous and more hydrated mixed copper oxide is obtained. Table 1 also shows a summary of the XPS binding energies for the conditions studied.

Additionally, the OH^- content effect on the morphology and chemical composition for anodized Cu surfaces was studied. Fig. 4a shows the potentiostatic j/t profiles recorded at E_{ap} = 10 V for different anodizing times of Cu foils at 5 °C in a 0.5 M KOH and 1% H_2O, in ethylene glycol containing 0.1% NH_4F electrolyte. Besides, Raman spectra (Fig. 4b) and FESEM images (Fig. 4c) for the anodized Cu foils are shown. The j/t profiles show current density values higher than the obtained at the same potential in 0.1 M KOH electrolytes (see Fig. 1b). The response is very reproducible showing three well-defined zones, which may be associated to changes in both the film composition (Fig. 4b) and morphology (Fig. 4c). At the initial stages of anodization ($t \leq 3$ min, zone I), the Raman spectrum shows only the presence of Cu_2O species at the surface, meanwhile for higher anodizing times (zones II and III), the characteristic CuO bands (296.0, 344.4 and 631.6 cm^{-1}) are also obtained. Furthermore, the porous morphology presents a progressive evolution with time (Fig. 4c) showing a strong enlargement in size of pores, which is attributed to the increase in the rate of chemical dissolution due to the higher KOH content.

Fig. 5 shows the $Cu2p_{3/2}$ (a), Cu LMM (b) and O1s (c) HRXPS spectra for an anodized Cu foil, applying 10 V during 6 min at 5 °C in a 0.5 M KOH and 1% v/v H_2O in ethylene glycol containing 0.1% w/v NH_4F electrolyte (see also Table 1 for summarized XPS and Raman signal assignments). The fit of the $Cu2p_{3/2}$ spectrum (Fig. 5a) gives us four contributions centered at 931.5 eV (6%), 933.2 eV (64%), 934.2 eV (17%) and 935.4 (13%); which are assigned to CuS, Cu + Cu_2O, CuO and $Cu(OH)_2$, respectively [14,15,27]. For this sample, sulfide presence may be due to contamination in the vacuum chamber. In agreement with these results, the deconvolution of the Cu LMM spectrum (Fig. 5b) shows 56% of Cu_2O (570.2 eV) and 44% Cu + CuO (568.4 eV). Complementary to this, the detailed O1s spectrum (Fig. 5c)

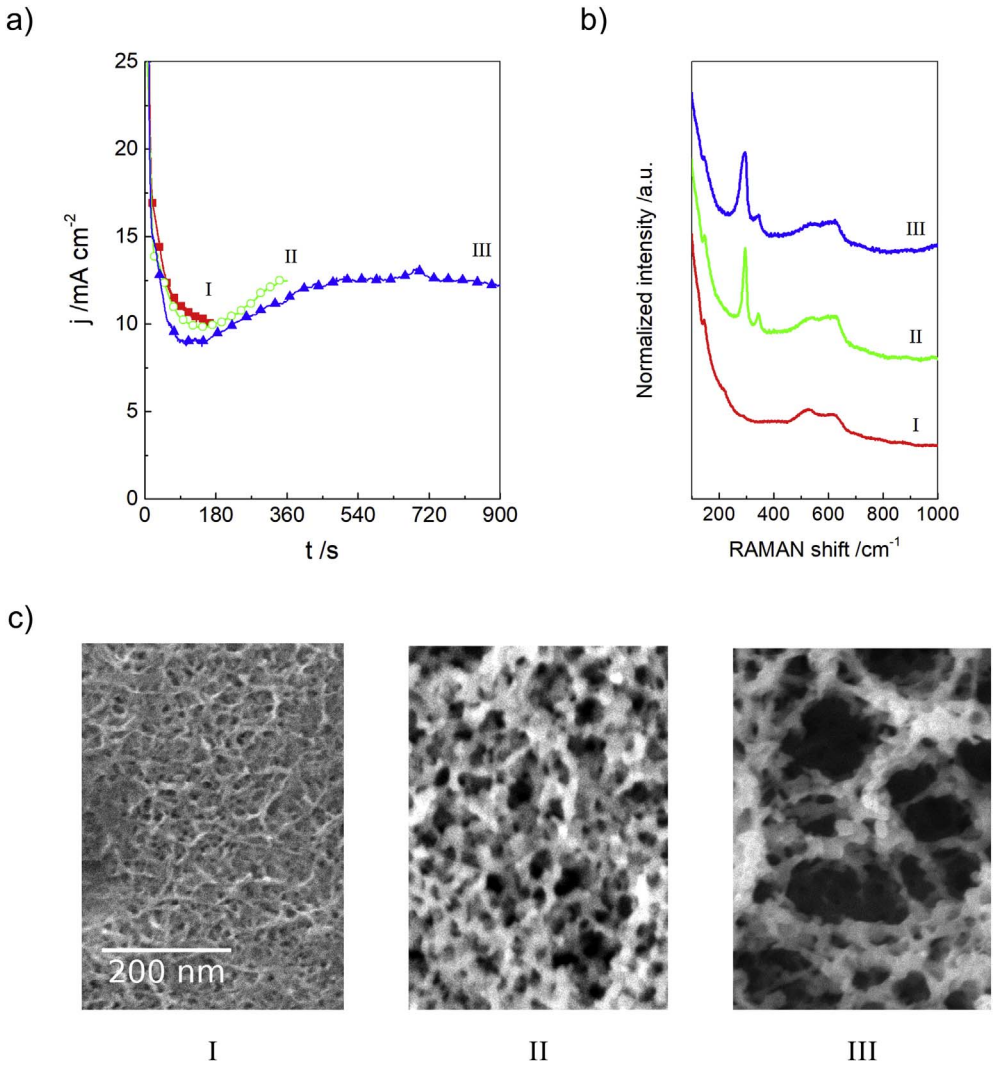

Fig. 4. a) Potentiostatic j/t profiles for the anodization at E_{ap} = 10 V during 3 min (I); 6 min (II) and 15 min (III) of Cu foils at 5 °C in a 0.5 M KOH and 1% H_2O in ethylene glycol containing 0.1% NH_4F electrolyte. b) Raman spectra for anodized Cu foils. c) FESEM images for I–III surfaces.

shows the three oxygen contributions assigned to CuO at 530.5 eV (22%); $Cu(OH)_2$ and adsorbed OH^- at 531.7 eV (58%) and adsorbed water at 532.9 eV (20%). These results indicate that the anodization in more concentrated hydroxyl ion electrolytes also promotes the oxidation to Cu(II), with $CuO/Cu_2O \approx 0.5$ (see Supporting information), and generates very hydrated rough films.

4. Discussion

The evidence shown in the previous section and summarized in Table 1, indicates that the anodization of copper in alkaline water/ethylene glycol media produces mainly Cu(II) species, according to previous reports [19,20]:

$$Cu(s) + 2OH^-(aq) \rightarrow CuO(s) + H_2O(l) + 2e^- \quad (1)$$

$$Cu(s) + 2OH^-(aq) \rightarrow Cu(OH)_2(s) + 2e^- \quad (2)$$

Instead, the Cu(I) species stabilizes by adding fluoride ions to the electrolytic bath, preventing the direct oxidation from Cu(0) to Cu(II). Previous reports indicate that Cl^- ions can be specifically adsorbed on the [100] crystalline metallic Cu face, thus promoting the formation and growth of Cu_2O layers [26]. Therefore, in the presence of fluoride the Cu(I) oxide formation, may take place according to:

$$Cu(sup) + F^-(aq) \rightarrow Cu - F(ad) + e^- \quad (3)$$

$$2Cu - F(ad) + 2OH^-(aq) \rightarrow Cu_2O(s) + H_2O(l) + 2F^- \quad (4)$$

On the other hand, in more alkaline media the subsequent oxidation to Cu(II) may come about, generating oxide/hydroxide films:

$$Cu_2O(s) + 2OH^-(aq) \rightarrow 2CuO(s) + H_2O(l) + 2e^- \quad (5)$$

$$Cu_2O(s) + 2OH^-(aq) + H_2O(l) \rightarrow 2Cu(OH)_2(s) + 2e^- \quad (6)$$

Additionally, as it has been previously reported [13], the generation of Cu(II) species is promoted by the increase in roughness of the underlying surface. Our microscopic analysis indicates that in more alkaline media, as the anodization time elapses significant changes in the surface morphology take place. The formation of the different nanostructures is related to local film dissolution produced by specific chemical species present in the electrolytic bath. It is well-known that Lewis bases as fluoride, hydroxyl and ammonia may act as complexing ligands for Cu(I) and Cu(II), generating different soluble species, e.g. $[Cu(NH_3)_2]^+$; $[Cu(NH_3)_5(OH_2)]^{2+}$; $[Cu(OH)_4]^{2-}$, and $[CuF]^+$ [14,20,28]. Among them, fluoride and hydroxyl ions may compete with the oxide formation (Eqs. 1 and 4), dissolving the layer or generating other fluorinated species as CuF_2.

5. Conclusions

We demonstrate that the anodization of copper in alkaline water/ethylene glycol media containing fluoride ions, generates different nanostructured oxide films. By modifying the anodization conditions (fluoride and OH^- concentration, voltage applied and anodization

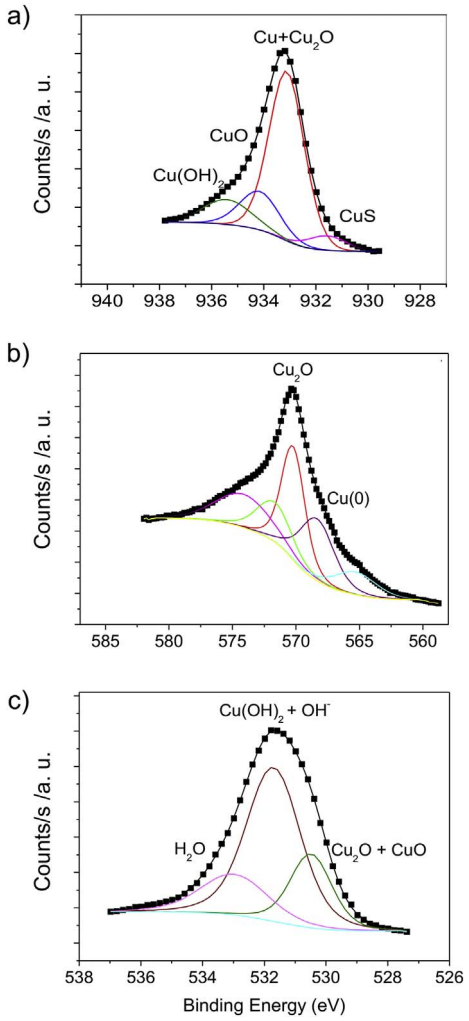

Fig. 5. $Cu2p_{3/2}$ (a), Cu LMM (b) and O1s (c) XPS spectra for a Cu foil anodized applying 10 V during 6 min at 5 °C in a 0.5 M KOH and 1% v/v H_2O in ethylene glycol containing 0.1% w/v NH_4F electrolyte.

time), nanofibrillar and nanoporous Cu_2O or $CuO/Cu(OH)_2$ films are obtained. The Raman and XPS measurements provide high quality information about the chemical states of the nanostructured films for the experimental conditions employed. In the absence of fluoride, the anodization of copper in alkaline water/ethylene glycol media produces mainly Cu(II) species meanwhile, in fluoride-containing media, Cu(I) oxide formation takes place. On the other hand, the subsequent oxidation to Cu(II) species occurs in more alkaline media promoted by the highly rough underlying surface for the higher voltages applied. These findings may allow tuning both the chemical species and the film morphology to generate specific nanostructured materials for potential use in a wide range of applications.

Acknowledgements

We thank project PMI-UAB 1301 of Universidad Andrés Bello for the financial support of this study and to the Iniciativa Científica Milenio (ICM) del Ministerio de Economía, Fomento y Turismo del Gobierno de Chile. G. del C Pizarro acknowledges to VRAC grant number L216-03 of the Universidad Tecnológica Metropolitana (UTEM). JS to Basal project USA 1555-Vridei 021741SP_PUBLIC Universidad de Santiago de Chile. OELP and MLT thank the financial support from the Consejo Nacional de Investigaciones Científicas y Técnicas of Argentina (CONICET) and the Secretaría de Ciencia y Tecnología (SECYT-UNC). Raman facilities at LANN, INFIQC-UNC/CONICET, Sistema Nacional de Microscopía - MINCyT, and FESEM microscopy facilities at LAMARX, FAMAF-UNC/CONICET, Sistema Nacional de Microscopía - MINCyT, are gratefully acknowledged.

Appendix A. Supplementary data

Supplementary data to this article can be found online at https://doi.org/10.1016/j.jelechem.2017.11.047.

References

[1] M. Velický, P.S. Toth, From two-dimensional materials to their heterostructures: an electrochemist's perspective, Appl. Mater. Today 8 (2017) 68–103.
[2] J. Wan, S.D. Lacey, J. Dai, W. Bao, Tuning two-dimensional nanomaterials by intercalation: materials, properties and applications, Chem. Soc. Rev. 45 (2016) 6742–6765.
[3] S. Khashan, S. Dagher, N. Tit, A. Alazzam, I. Obaidat, Novel method for synthesis of Fe_3O_4@TiO_2 core/shell nanoparticles, Surf. Coat. Technol. 322 (2017) 92–98.
[4] M.A. Awad, N.M.A. Hadia, Copper oxide nanocrystallites fabricated by thermal oxidation of pre-sputtered copper films at different temperatures and under oxygen and argon flows, Optik 142 (2017) 334–342.
[5] Y. Mei, M. Yuxiao, L. Jianhua, L. Xinjie, L. Songmei, L. Shenyao, Sub-coherent growth of ZnO nanorod arrays on three-dimensional graphene framework as one-bulk high-performance photocatalyst, Appl. Surf. Sci. 390 (2016) 266–272.
[6] D. Kowalski, D. Kim, P. Schmuki, TiO_2 nanotubes, nanochannels and mesosponge: self-organized formation and applications, Nano Today 8 (2013) 235–264.
[7] C. Gattinoni, A. Michaelides, Atomistic details of oxide surfaces and surface oxidation: the example of copper and its oxides, Surf. Sci. Rep. 70 (2015) 424–447.
[8] D. Tahir, S. Tougaard, Electronic and optical properties of Cu, CuO and Cu_2O studied by electron spectroscopy, J. Phys. Condens. Matter 24 (2012) 175002–175010.
[9] K.P. Musselman, A. Wisnet, D.C. Iza, H.C. Hesse, C. Scheu, J.L. MacManus-Driscoll, L. Schmidt-Mende, Strong efficiency improvements in ultra-low-cost inorganic nanowire solar cells, Adv. Mater. 22 (2010) E254–E258.
[10] K. Akimoto, S. Ishizuka, M. Yanagita, Y. Nawa, G.K. Paul, T. Sakurai, Thin film deposition of Cu_2O and application for solar cells, Sol. Energy 80 (2006) 715–722.
[11] A.S. Aiswarya Raj, V. Biju, Nanostructured CuO: facile synthesis, optical absorption and defect dependent electrical conductivity, Mater. Sci. Semicond. Process. 68 (2017) 38–47.
[12] H.W. Zhang, X. Zhang, H.Y. Li, Z.K. Qu, S. Fan, M.Y. Ji, Hierarchical growth of Cu_2O double tower-tip-like nanostructures in water/oil microemulsion, Cryst. Growth Des. 7 (2007) 820–824.
[13] J.J. Diaz Leon, D.M. Fryauf, R.D. Cormia, Min-Xian Max Zhang, K. Samuels, R. Stanley Williams, N.P. Kobayashi, Reflectometry – ellipsometry reveals thickness, growth rate, and phase composition in oxidation of copper, ACS Appl. Mater. Interfaces 8 (2016) 22337–22344.
[14] I. Platzman, R. Brener, H. Haick, R. Tannenbaum, Oxidation of polycrystalline copper thin films at ambient conditions, J. Phys. Chem. C 112 (2008) 1101–1108.
[15] I. Platzman, C. Saguy, R. Brener, R. Tannenbaum, H. Haick, Formation of ultrasmooth and highly stable copper surfaces through annealing and self-assembly of organic monolayers, Langmuir 26 (2010) 191–201.
[16] X. Wu, H. Bai, J. Zhang, F. Chen, G. Shi, Copper hydroxide nanoneedle and nanotube arrays fabricated by anodization of copper, J. Phys. Chem. B 109 (2005) 22836–22842.
[17] Duc-Duong La, Y.P. Sung, C. Young-Wook, K. Yong-Shin, Wire-like bundle arrays of copper hydroxide prepared by the electrochemical anodization of Cu foil, Bull. Kor. Chem. Soc. 31 (2010) 2283–2288.
[18] S. Sahoo, S. Husale, B. Colwill, Toh-Ming Lu, S. Nayak, P.M. Ajayan, Electric field directed self-assembly of cuprous oxide nanostructures for photon sensing, ACS Nano 12 (2009) 3935–3944.
[19] N.K. Allam, C.A. Grimes, Electrochemical fabrication of complex copper oxide nanoarchitectures via copper anodization in aqueous and non-aqueous electrolytes, Mater. Lett. 65 (2011) 1949–1955.
[20] W.J. Stepniowski, S. Stojadinović, R. Vasilić, N. Tadić, K. Karczewski, S.T. Abrahami, J.G. Buijnsters, J.M.C. Mol, Morphology and photoluminescence of nanostructured oxides grown by copper passivation in aqueous potassium hydroxide solution, Mater. Lett. 198 (2017) 89–92.
[21] D.P. Oyarzún, E.C. Muñoz, R.A. Córdova, O.E. Linarez Pérez, R.G. Henríquez, M. López Teijelo, H. Gómez, Morphological, electrochemical and photoelectrochemical characterization of nanotubular TiO_2 synthetized electrochemically from different electrolytes, J. Solid-State Electrochem. 15 (2011) 2265–2275.
[22] W. Wang, O. Varghese, M. Paulose, C.A. Grimes, Q. Wang, E. Dickey, A study on the growth and structure of titania nanotubes, J. Mater. Res. 19 (2004) 417–422.
[23] J.C. Hamilton, J.C. Farmer, R.J. Anderson, In situ Raman spectroscopy of anodic films formed on copper and silver in sodium hydroxide solution, J. Electrochem. Soc. 133 (1986) 739–745.
[24] S.T. Mayer, R.H. Muller, An in situ Raman spectroscopy study of the anodic oxidation of copper in alkaline media, J. Electrochem. Soc. 139 (1992) 426–434.
[25] M. Ivanda, D. Waasmaier, A. Endriss, J. Ihringer, A. Kirfel, W. Kiefer, Low-temperature anomalies of cuprite observed by Raman spectroscopy and X-ray powder diffraction, J. Raman Spectrosc. 28 (1997) 487–493.
[26] M.J. Siegfried, Kyoung-Shin Choi, Elucidating the effect of additives on the growth and stability of Cu_2O surfaces via shape transformation of pre-grown crystals, J. Am. Chem. Soc. 128 (2006) 10356–10357.
[27] G.G. Totir, G.S. Chottiner, C.L. Gross, D.A. Scherson, XPS studies of the chemical and electrochemical behavior of copper in anhydrous hydrogen fluoride, J. Electroanal. Chem. 532 (2002) 151–156.
[28] S. Kotrlý, L. Šůcha, Handbook of Chemical Equilibria in Analytical Chemistry, Ellis Horwood Limited, Halsted Press, John Wiley & Sons, New York, 1985.